Acta of Bioengineering and Biomechanics
Vol. 24, No. 4, 2022

Original paper
DOI: 10.37190/ABB-02175-2022-01

Modern methods of surface modification for new-generation titanium alloys

JULIA LISOŃ-KUBICA[1]*, ANNA TARATUTA[1], KAROLINA GOLDSZTAJN[1], MAGDALENA ANTONOWICZ[1], WITOLD WALKE[1], ANETA DYNER[2], MARCIN BASIAGA[1]

[1] Silesian University of Technology, Faculty of Biomedical Engineering, Department of Biomaterials and Medical Devices Engineering, Zabrze, Poland.
[2] Fabryka Narzędzi Medycznych CHIRMED Marcin Dyner, Rudniki, Poland.

The constantly growing need for the use of implants in osteotomy is mainly due to the aging population and the need for long-term use of this type of biomaterials. Improving implant materials requires the selection of appropriate functional properties. Currently used titanium (Ti) alloys, such as Ti6Al4V and Ti6Al7Nb, are being replaced by materials with better biocompatibility, such as vanadium(V) or niobium (Nb), allowing for creation of the so-called new generation alloys. These new alloys, with the incorporation of zirconium (Zr), iron, and tantalum, possess Young's modulus close to that of a bone, which further improves the improves the biomaterial's. biocompatibility. This article describes the atomic layer deposition (ALD) method and its possible applications in the new generation of titanium alloys for biomedical applications. Also, the exemplary results of tin oxide (SnO_2) thin coatings deposited by ALD and physical vapor deposition (PVD) methods are presented. This study aimed to evaluate the physicochemical properties of a Ti13Nb13Zr alloy used for elements in the skeletal system. As the temperature and the number of cycles vary, the results demonstrate that the surface area of the samples changes. The uncoated Ti13Nb13Zr alloy exhibits hydrophilic properties. However, all coated specimens improve in this respect and provide improved clinical results. after the applied modification, the samples have a smaller contact angle, but still remain in the range of 0–90°, which makes it possible to conclude that their nature remains hydrophilic. Coating the specimens decreased the mineralization risk of postoperative complications. As a result, the biomaterials demonstrated improved effectiveness, decreased complication indicators, and improved patient well-being.

Key words: *titanium alloy, atomic layer deposition, physical vapor deposition, surface modification, antibacterial coatings*

1. Introduction

Bone implants generally consist of light metals or alloys such as titanium (Ti) and Ti alloys. Due to economic growth and technological advancements, the number of elderly people seeking to remediate the unsuccessful replacement of organs with improved products is growing rapidly. It is estimated that 70–80% of biomedical devices are made of metallic material. Metal implants are extremely effective in rebuilding damaged hard tissue. As an individual's lifespan increases, the demand for biomaterials grows on a huge scale. Ti alloys are now widely used due to their remarkable properties such as corrosion resistance, non-toxicity and cytocompatibility. However, the most prominent Ti alloys, Ti6Al4V and Ti6Al7Nb, are being replaced because aluminum (Al) or cytotoxic vanadium(V) may cause allergies, so the authors do not recommend to use them in the human body in case of fear of allergens [9], [11]–[13], [17]. Niobium (Nb) and Zirconium (Zr) are more biocompatible and do not result in cytotoxicity and neurological diseases, caused by the elements V and Al, respectively. Nevertheless, Ti-based alloys seem to have relatively low abrasion resistance [16]. Currently, more biocompatible materials are used [3]. In the case of new-generation alloy materials, those incorporating zircon, iron and

* Corresponding author: Julia Lisoń-Kubica, Silesian University of Technology, Faculty of Biomedical Engineering, Department of Biomaterials and Medical Devices Engineering, ul. Roosevelta 40, 41-800 Zabrze. E-mail: julia.lison@polsl.pl
Received: September 29th, 2022
Accepted for publication: April 11th, 2023

tantalum have Young's moduli of a values close to those of the bone [8]. Biomaterials used for bone implants are characterized by good corrosion resistance, appropriate mechanical and electrical properties, high metallurgical quality, surface homogeneity, biocompatibility, abrasion resistance, and relatively low production costs.

To maintain optimal mechanical stability during implantation and to improve the physicochemical properties, various surface modification methodologies are used [3]. Currently, the application of nanolayers is one of the most popular surface modifications. Nanoparticles can be deposited on the surface of implants to change their surface chemistry. For example, silver (Ag) nanoparticles were initially used to coat orthopedic pins to prevent bacterial colonization, and dispersed Ag nanoparticles can be used in polymethyl methacrylate (PMMA) as bone cement. In addition, nanoscale Ti sol–gel layers with deposited Ag, zinc (Zn), mercury (Hg), copper (Cu), cobalt (Co) and aluminium (Al) metal salts deposited on Ti surfaces were used. Bone implants with modified Ti and Zr oxide (TiO_2 and ZrO_2, respectively) nanocrystalline coatings were tested for osseointegration and antibacterial activity [4]. There are a variety of thin film deposition techniques collectively referred to as physical vapor deposition (PVD) or atomic layer deposition (ALD). ALD coats materials with atomic-scale precision. This surface modification is about self-limiting chemical reactions on surfaces, therefore, yielding atomic-level control over the film thickness and composition without the need for line-of-site access to the precursor source, for example, Al Oxide (Al_2O_3), TiO_2, Zn, tin (Sn), Zn oxide (ZnO) or Sn oxide (SnO_2) application [1], [5]. The study aimed to assess the physicochemical and mechanical properties of the modified Ti13Nb13Zr alloy, considered to be a material with a high level of biocompatibility and Young's modulus of closer value to bone tissue, which is particularly important in the context of treating the skeletal system and the process of osseointegration.

2. Materials and methods

Ti alloy (Ti13Nb13Zr) samples obtained from a bar with a 14 mm diameter were used in the study. The samples were ground and electropolished. The grinding was carried out by successively changing gradations of paper (i.e., 500, 1200, and 2000 grit). Electrochemical polishing was performed using a solution of phosphate sulfate. Subsequently, the SnO_2 coating was applied to the polished samples using ALD. Sn(IV) chloride (Cl), anhydrous (99.99-Sn%) PURATREM was used as the Sn precursor (Table 1), which reacted with deionized water, allowing for the deposition of the thin films.

Table 1. Chemical properties of PURATREM

Molecular weight:	260.50
Formula:	Cl_4Sn
Purity:	99.99-Sn%
Color/Form:	colorless liq.
Melting point:	–33 °C
Boiling point:	114.1 °C
HS code:	2827.39.2500

The application process was carried out at 100 °C for 500 cycles. Then, the polished samples underwent PVD by the SnO_2 coating also. The precursor used was 3 mm thick with a 50.8 mm diameter (99.9% pure, LOT013736 Testbourne Ltd). Argon was used to generate the plasma for PVD. The gas (argon) was introduced at a power rate of 25%. To assess the suitability of the proposed surface modification method, the authors proposed a series of tests.

Potentiodynamic method

In the first stage, the pitting corrosion resistance tests were performed using the potentiodynamic method. The reference electrode was Ag/AgCl 3M potassium Cl (KCl), while the auxiliary rod was platinum. The scan rate was set to 3 mV/s. These tests enabled the analysis of the structural characteristics of the coatings such as possible defects, lack of sealing, substrate reactivity, and the presence of barrier properties involving the electrolyte. Tests of the resistance to the pitting corrosion were carried out in saline solution (phosphate buffered saline, PBS) to create an environment similar to the natural tribological conditions present in the human body.

Electrochemical impedance spectroscopy (EIS)

To obtain additional information about the physicochemical properties of the analyzed samples' surfaces, electrochemical impedance spectroscopy (EIS) was also performed. The measurements were carried out using the Auto Lab measurement system equipped with a 302N PGSTAT FRA2 (Frequency Response Analyser) module. The measurement system enabled experiments in the frequency range of 10^{-3}–10^4 Hz. In the study, the impedance spectra were collected and the obtained measurements were fitted to the equivalent circuit. On this basis, the resistance (R) and ca-

pacitance (C) of the analyzed system were determined. Impedance spectra of the analyzed systems were presented in the form of Nyquist diagrams for different values of frequency as well as in the form of Bode diagrams. The obtained EIS spectra were interpreted after adjusting the least squares method to the equivalent electrical system.

Scratch test

The scratch test involved creating a scratch with the use of a penetrator – i.e., a Rockwell diamond cone – with a gradual increase in the normal force load applied to the penetrator. The tests were performed with an increased loading force from 0.03–30 N using the following operating parameters: 10 N/min loading speed, 1 mm/min table speed, and an ~3 mm scratch length.

Tribological testing

The tribological wear test was conducted to study the friction, wear and surface adhesion. The abrasion tests were performed using a tribometer, with the application of a 5 N force load on all of the samples, for which the following courses of the abrasion coefficient were obtained. The tribological tests were carried out using the technical parameters presented in Table 2. Steel and Al_2O_3 balls with a diameter of 6 mm were used during these tests as counter-samples in the friction pairs.

Table 2. Technical parameters of the test

Parameter	Friction pair
	Al_2O_3 ball- disc Ti13Nb13Zr Steel ball- disc Ti13Nb13Zr
Load [N]	5
Linear speed [cm/s]	2.83
Cycle [–]	1000
Frequency [Hz]	80

Scanning electron microscope imaging

Microscopic observations following tribological testing were performed using scanning electron microscopy (SEM, TESCAN VEGA). The tests were carried out in high vacuum conditions at a voltage of 15 kV, using a backscattered electron (BSE) detector. The images taken at different magnifications enabled the evaluation of the debris traces created during the wear test.

Wettability

To determine the wettability of the sample surface, a contact angle method was performed on the selected samples using the sitting drop method. Measurements of the contact angle of each surface were made using 1.5 mm^3 of distilled water and applying the Surftens Universal optical goniometer (OEG). The Surftens 4.5 computer software was used for the analysis of the recorded drop images. The measurements were performed at room temperature (23 ± 1 °C) over 60 s with a sampling rate of 1 Hz. The obtained data showed the different physicochemical properties of the antibacterial films generated under surface modification.

3. Results

Potentiodynamic method

After surface preparation, grinding, and polishing after the SnO_2 coating was applied using ALD technology and PVD methods, the samples were subjected to potentiodynamic tests to investigate the resistance to pitting corrosion in saline solution (PBS). The results of potentiodynamic tests are displayed in the polarization curves (Fig. 1).

The values corresponding to the corrosion potential (Potential E) and current density are presented in

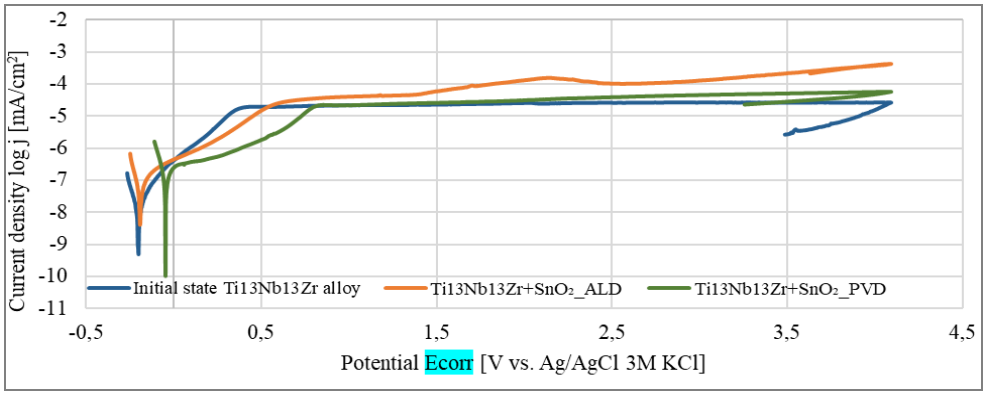

Fig. 1. Potentiodynamic curves of the initial state of the Ti13Nb13Zr and the alloy with coatings

Table 3. Analyzing the sample polarization curves reveals that the higher polarization resistance (R_p) values, indicating improved corrosion resistance, occur for Ti13Nb13Zr with SnO_2 coatings compared to the initial state Ti13Nb13Zr sample. The performed tests made it possible to determine the influence of the surface treatment on corrosion resistance. Moreover, the surface modification had an impact on the measurement parameters. The parameter values that relate to the corrosion resistance of the tested samples correspond to the corrosion potential (E_{corr}) and current density presented in Fig. 1.

Table 3. Results of the potentiodynamic tests

Sample	Polarization data	
	E_{corr} [mV]	R_p [kΩ·cm^2]
Ti13Nb13Zr	–200	1.15
Ti13Nb13Zr+SnO_2_ALD	–211	2.21
Ti13Nb13Zr+SnO_2_PVD	–50	1.19

Electrochemical impedance spectroscopy (EIS)

To identify the nature of the generated SnO_2 coating on the surface of the Ti13Nb13Zr samples, measurements using EIS were performed in the subsequent stage of studies. Typical impedance spectra recorded for test specimens of the Ti13Nb13Zr + SnO_2 sample prepared using ALD and PVD methods are presented in Figs. 3 and 4.

The obtained electrical properties determined using the basis of the recorded spectra are summarized in Table 4.

In both Nyquist diagrams near the origin of the coordinate system, fragments of semicircles distorted to varying degrees are revealed which transform into a linear relationship between the imaginary (Z″) and real (Z′) components of the impedance in some cases (Figs. 1–4). The conducted tests indicate that the impedance modulus of the systems, regardless of the type of substrate and the parameters of the SnO_2 coating deposition via the PVD method, decreases with increasing frequency. The process of applying the coating to the Ti13Nb13Zr substrate resulted in lower electrochemical stability of the surface layer, as evidenced by the relatively lower value of the charge transfer resistance (R_{ct}). The obtained shapes of the polished samples with the SnO_2 coating indicate the presence of a porous oxide layer as a result of the interaction with the PBS solution. In the case of these

Table 4. EIS results

Sample	R_s [Ω·cm^2]	C_{ad} [μF]	R_{ad} [Ω·cm^2]	C_{pore} [μF]	R_{pore} [kΩ·cm^2]	CPE_{pore}		C_{dl} [μF]	R_{ct} [kΩ·cm^2]	CPE_{dl}		E_{OCP} [mV]
						Y_0 [Ω^{-1}cm^{-2}s^{-n}]	n			Y_0 [Ω^{-1}cm^{-2}s^{-n}]	n	
Ti13Nb13Zr	138	–	–	–	164	$0.1888\cdot10^{-4}$	0.88	–	347	$0.2195\cdot10^{-4}$	0.93	–257
Ti13Nb13Zr +SnO_2_PVD		9	6184	17	88	–	–	160	141	–	–	–188
Ti13Nb13Zr +SnO_2_ALD		–	–	–	–	–	–	–	4320	$0.2348\cdot10^{-4}$	0.94	–222

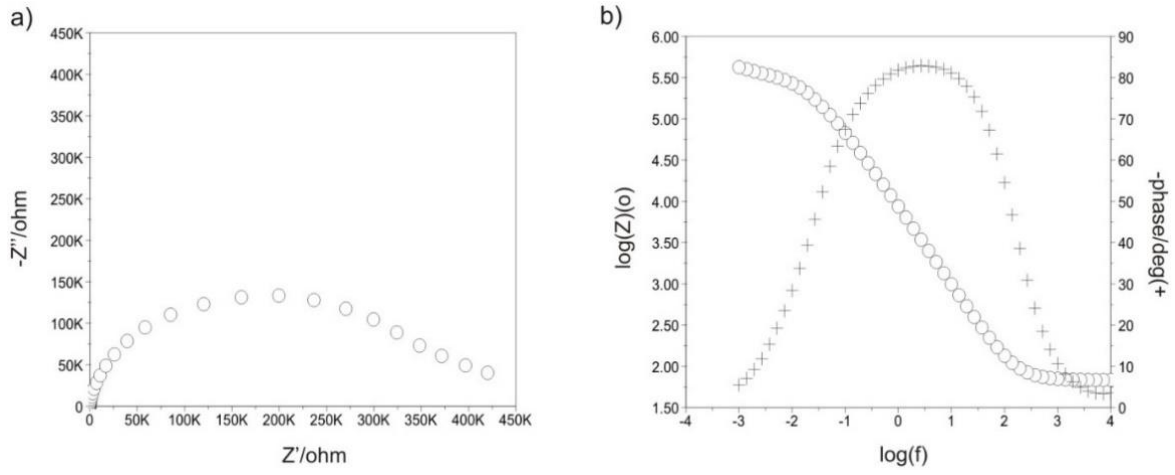

Fig. 2. Impedance spectra for the initial state of the Ti13Nb13Zr alloy are illustrated using: a) Nyquist and b) Bode diagrams

samples, a change in the angle of inclination of the rectilinear section in the low-frequency part of the spectrum was observed. Initially, the angle was characteristic for the Warburg impedance (45°) but then changed to an angle characteristic for membrane-type layers. This can be explained by the formation of a biofilm at the interface between the SnO_2 coating and the PBS solution. According to this model, the two *R* and CPE elements are connected in series with the solution resistance (R_s) (Fig. 5a). This is probably due to the partial degradation of the SnO_2 coating in the surface sublayer with the simultaneous formation of membrane-type films in the inner layer (adsorption layer) (Fig. 5b). The passive film and electrical double layer are assumed to show on ideal capacitive behavior or non-ideal capacitive behavior. Pore resistance (R_{pore}) and constant phase element of the pore (CPE_{pore}) are representative of the electrical porous layer whereas R_{ct} and constant phase element of the double layer (CPE_{dl}) represent the resistive and non-ideal capacitive behavior of the passive film (double layer).

In turn, the best match of the model spectra to the impedance spectra determined experimentally in the PBS solution for samples with the SnO_2 coating deposited by the ALD method is provided by a simple equivalent circuit with a one-time constant consisting of four electrical elements (Fig. 5c). In this circuit, R_s models the resistance of the electrolyte, i.e., PBS solution, R_{ct} characterizes the resistance of electric charge transfer at the interface between the SnO_2 shell and the PBS solution, and CPE_{dl} describes the electrical properties of the double layer at the interface of these phases. The auxiliary electric system (Fig. 5) was used for the analysis of the experimental-

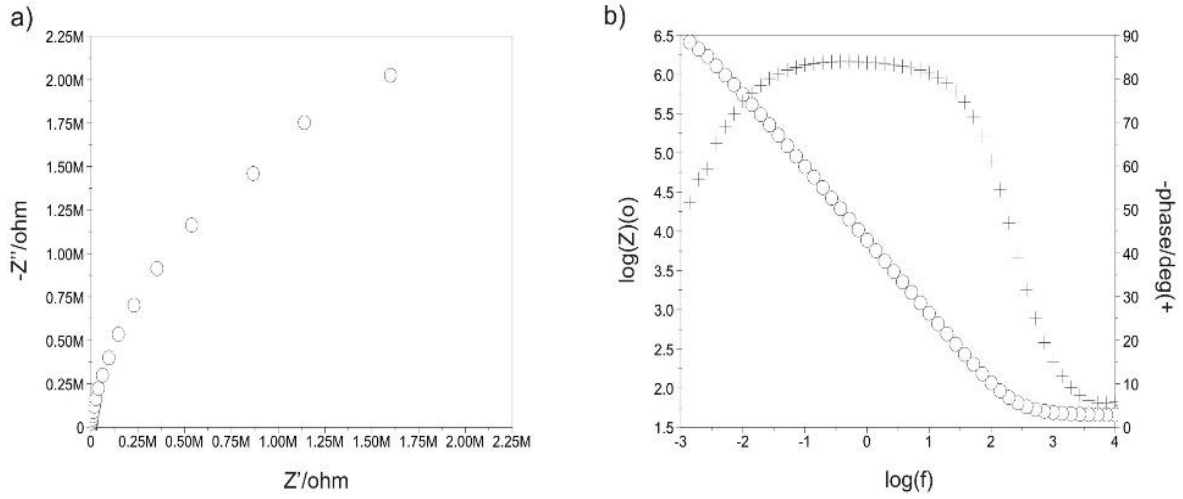

Fig. 3. Impedance spectra for the Ti13Nb13Zr alloy with the SnO_2 coating modified by the ALD method (Ti13Nb13Zr+SnO_2_ALD) illustrated using: a) Nyquist and b) Bode diagrams

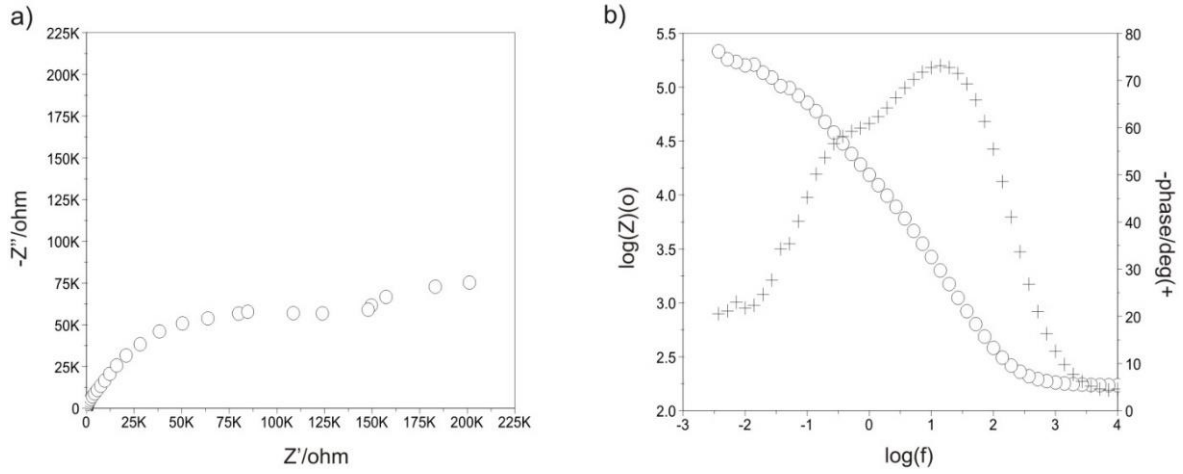

Fig. 4. Impedance spectra for the Ti13Nb13Zr alloy with the SnO_2 coating modified by the PVD method (Ti13Nb13Zr+SnO_2_PVD) illustrated using: a) Nyquist and b) Bode diagrams

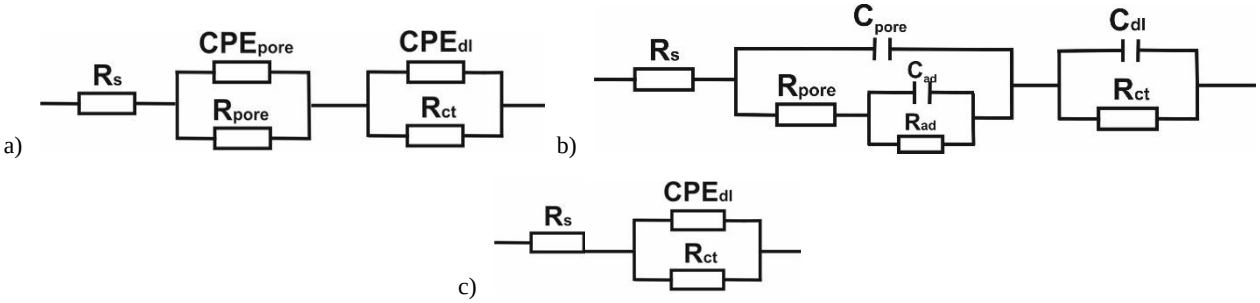

Fig. 5. Electrical equivalent circuits for the corrosion system consisting of Ti13Nb13Zr alloy in PBS solution for: a) Ti13Nb13Zr, b) Ti13Nb13Zr+SnO_2_PVD, and c) Ti13Nb13Zr+SnO_2_ALD samples

ly determined impedance spectra of the corrosive system for Ti13Nb13Zr alloy and Ti13Nb13Zr with SnO_2 coatings prepared using ALD and PVD.

Scratch test

Next, the scratch test was conducted, and the differences in the critical force (Figs. 6, 7, Table 5), which is a measure of adhesion, were recorded. The average force of the coating damage after the complete destruction of the Ti13Nb13Zr sample with the SnO_2_ALD coating (Ti13Nb13Zr+SnO2_ALD) was observed with the critical load (Lc_3) equals: 6.14 N. On the other hand, chipping-Lc_2 and complete destruction-Lc_3 have been registered in the case of the Ti13Nb13Zr sample with the SnO_2 coating modified by the PVD method (Ti13Nb13Zr +SnO_2_PVD).

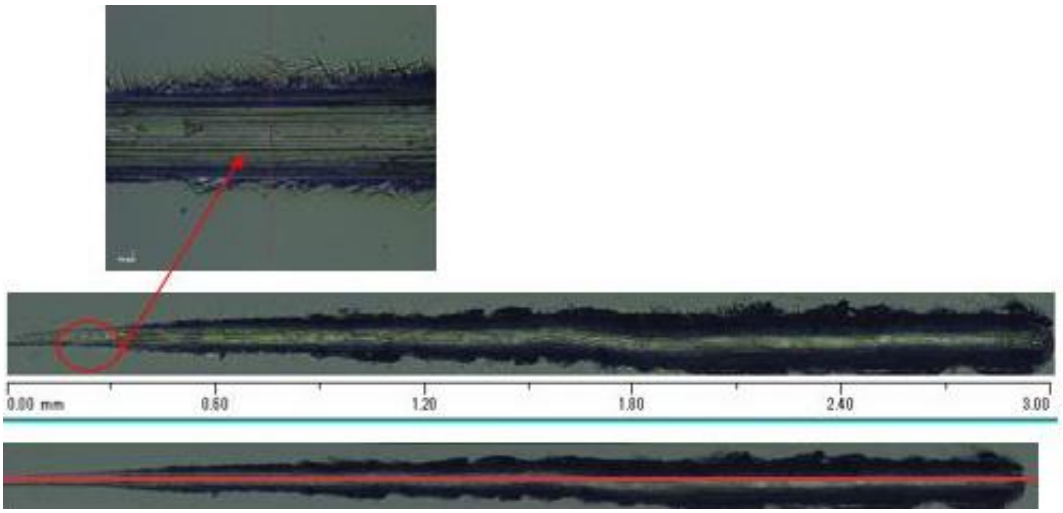

Fig. 6. Optical micrographs of the adhesion tests for a Ti13Nb13Zr sample with the SnO_2 coating modified by the ALD method (Ti13Nb13Zr+SnO_2_ALD)

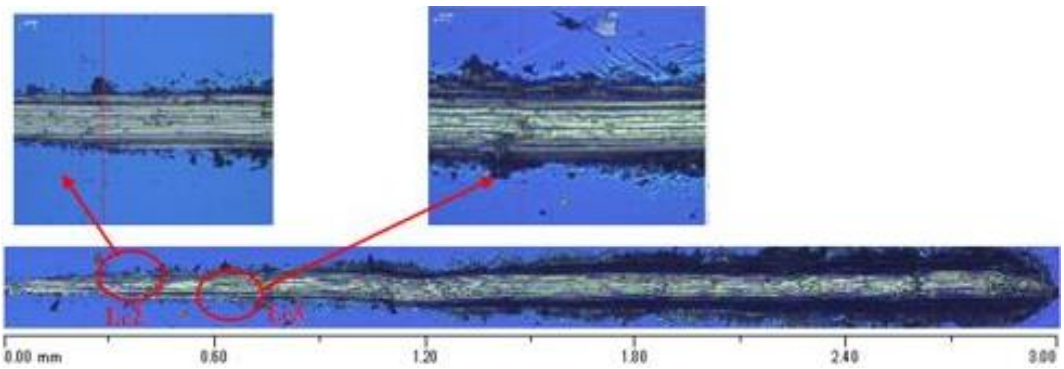

Fig. 7. Optical micrographs of the adhesion tests for a Ti13Nb13Zr sample with the SnO_2 coating modified by the PVD method (Ti13Nb13Zr +SnO_2 _PVD)

Table 5. Results of the scratch test

Method of sample surface preparation	Coating damage	Average force *F* [N]
Ti13Nb13Zr+SnO_2_ALD	Complete destruction of Lc_3	6.14
Ti13Nb13Zr+SnO_2_PVD	Chip of Lc_2	3.57
	Complete destruction of Lc_3	4.64

Complete destruction of the coating was observed in every sample analyzed. The higher average force for Ti13Nb13Zr+SnO_2_ALD samples makes it possible to conclude that ALD samples are characterized by better adhesion to the coating than Ti13Nb13Zr+SnO_2_PVD samples. Additionally, there was no acoustic emission signal for the samples, which proves that the bonding energy between the coating and the substrate was too low. Moreover, SEM observations conducted after performing the scratch test revealed complete destruction (Lc_3) (Fig. 8).

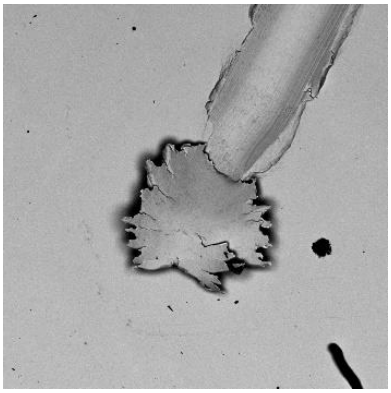

Fig. 8. SEM micrograph of the Ti13Nb13Zr+SnO_2_ALD sample surface after the scratch test (SEM area taken at 400×)

Tribological testing

For samples with SnO_2 coatings, the coefficient of friction was decreased and the abrasion resistance improved. Following the application of the coating, the friction coefficient decreased to a greater extent for Ti13Nb13Zr+SnO_2_ALD and Ti13Nb13Zr+SnO_2_PVD samples compared to the initial state Ti13Nb13Zr samples. The average coefficients of the abrasion for the tested samples are summarized in Figs. 9 and 10. Tribological test results performed using an Al_2O_3 ball.

To evaluate the tribological properties of the tested materials, friction tests were performed and summarized (Figs. 9, 10). The friction coefficient (μ) of the test elements depends on the types of materials and friction pairs. After modification by SnO_2 coating by ALD and PVD method, the friction coefficient

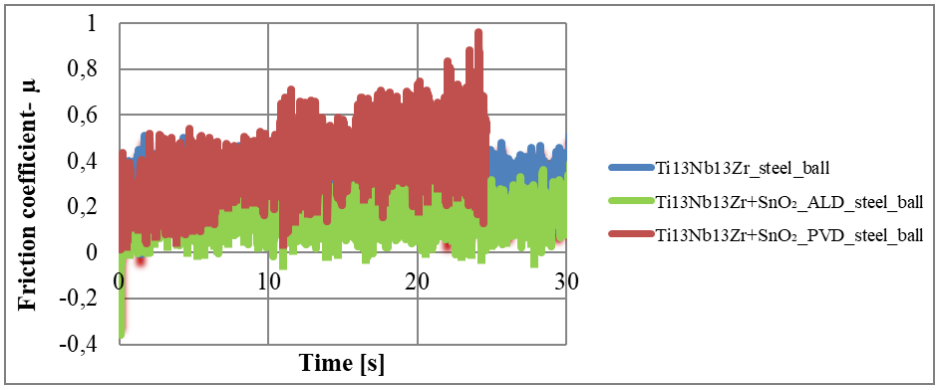

Fig. 9. Tribological test results performed using a steel ball

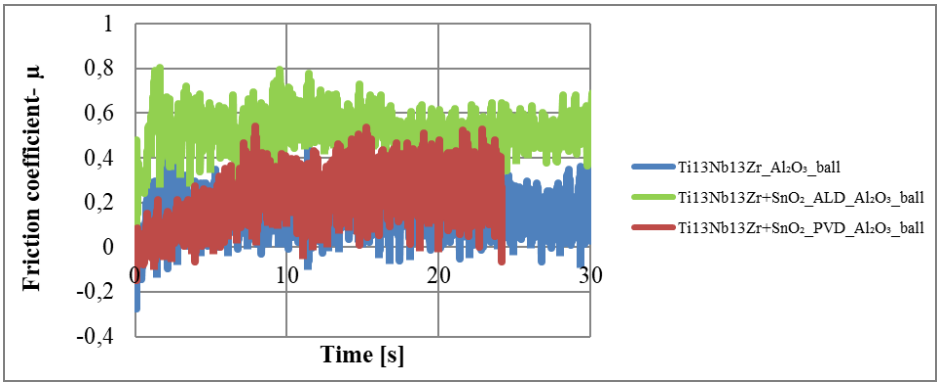

Fig. 10. Tribological test results performed using an Al_2O_3 ball

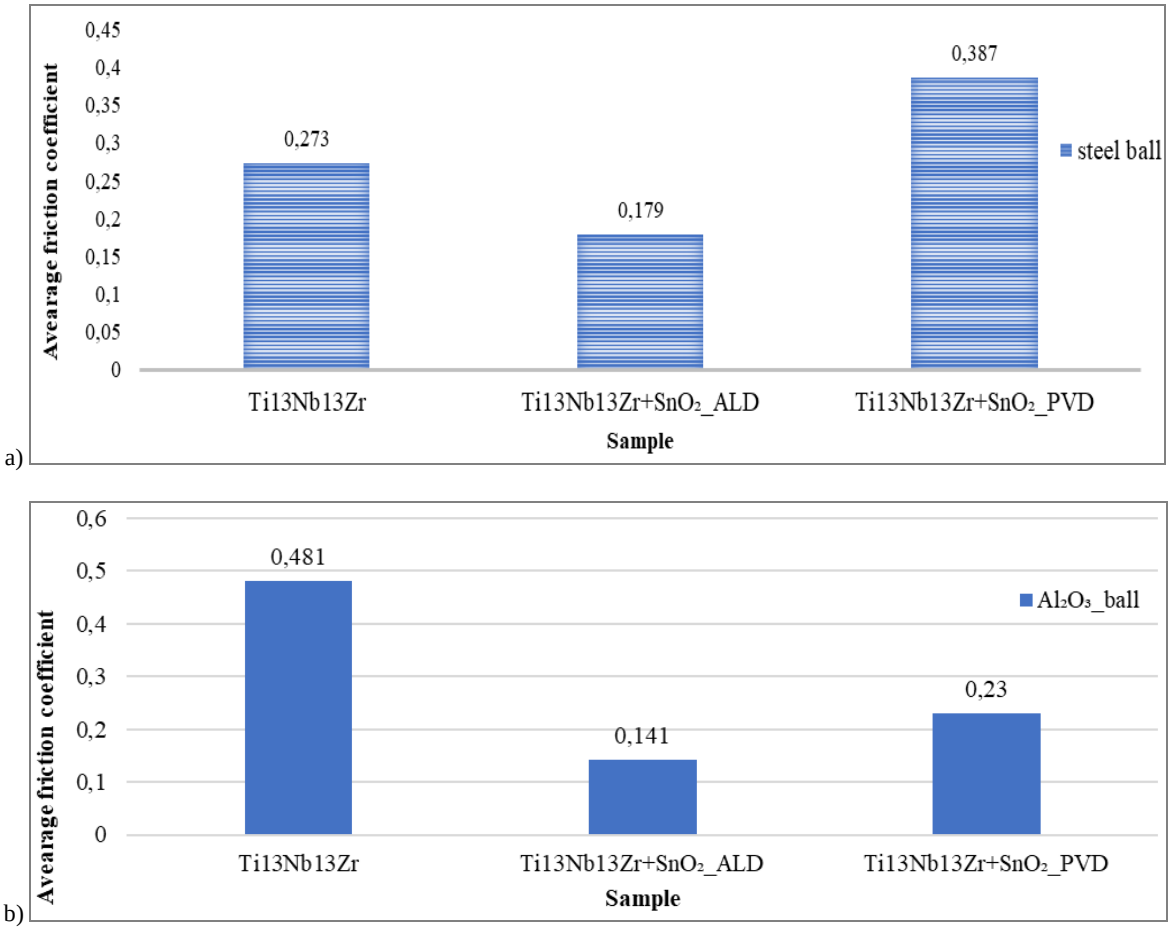

Fig. 11. The average coefficient of friction, μ, values for the Ti13Nb13Zr alloy and surface-modified samples were determined using: a) sample-steel ball and b) sample-Al_2O_3 ball friction pairs

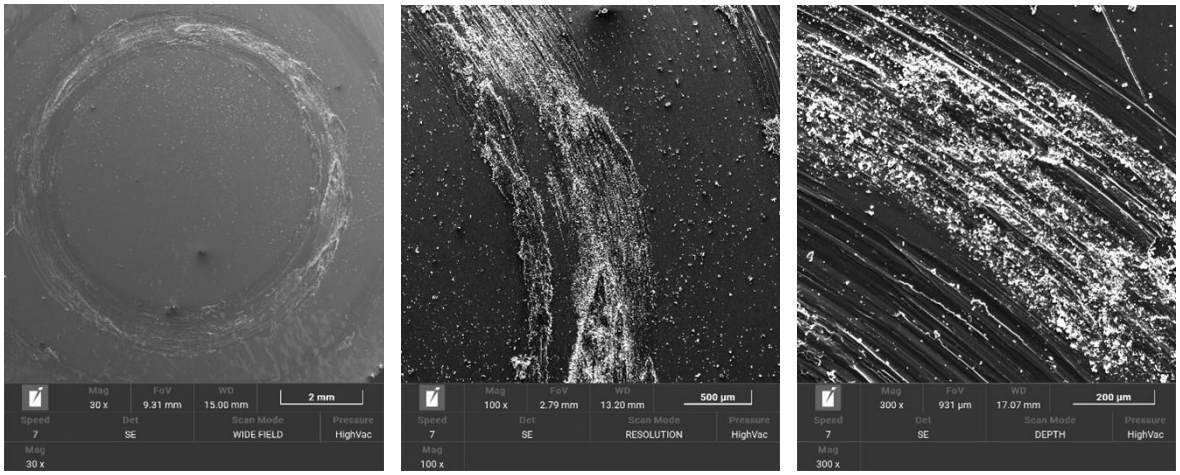

a) b) c)

Fig. 12. The surface of the Ti13Nb13Zr alloy with the SnO_2 coating modified by the ALD method after the friction pair abrasion test: Ti13Nb13Zr+SnO_2_ALD -Al_2O_3 ball, with SEM magnifications of a) 30×, b) 100×, and c) 300×

decreased in using Al_2O_3 ball during examination. The similar dependency of the tribological characteristics was not obtained for the material combination of Ti13Nb13Zr with SnO_2 coatings with steel ball like counter sample. Moreover, the SEM observation was conducted after tribological testing which revealed trace abrasions with Al_2O_3 and steel balls (Fig. 11).

Moreover, the SEM observations conducted after tribological testing revealed traces of abrasion with Al_2O_3 (Figs. 12 and 13) and steel balls (Figs. 14 and 15).

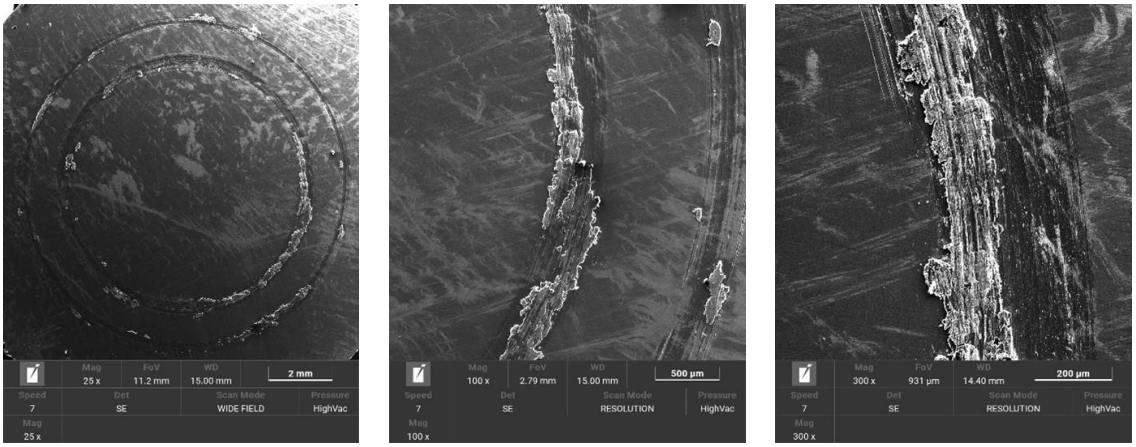

a) b) c)

Fig. 13. The surface of the Ti13Nb13Zr alloy with the SnO_2 coating modified by the ALD method after the friction pair abrasion test: Ti13Nb13Zr+Sn -steel ball, with SEM magnifications of a) 25×, b) 100×, and c) 300×

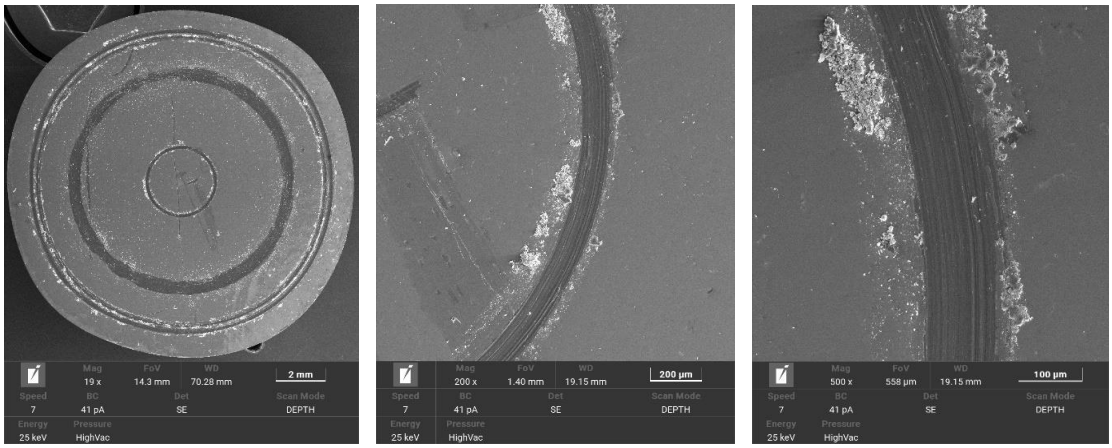

a) b) c)

Fig. 14. The surface of the Ti13Nb13Zr alloy with the SnO_2 coating modified by the PVD method coating after the friction pair abrasion test: Ti13Nb13Zr+SnO_2-Al_2O_3 ball, with SEM magnifications of: a) 19×, b) 200×, and c) 500×

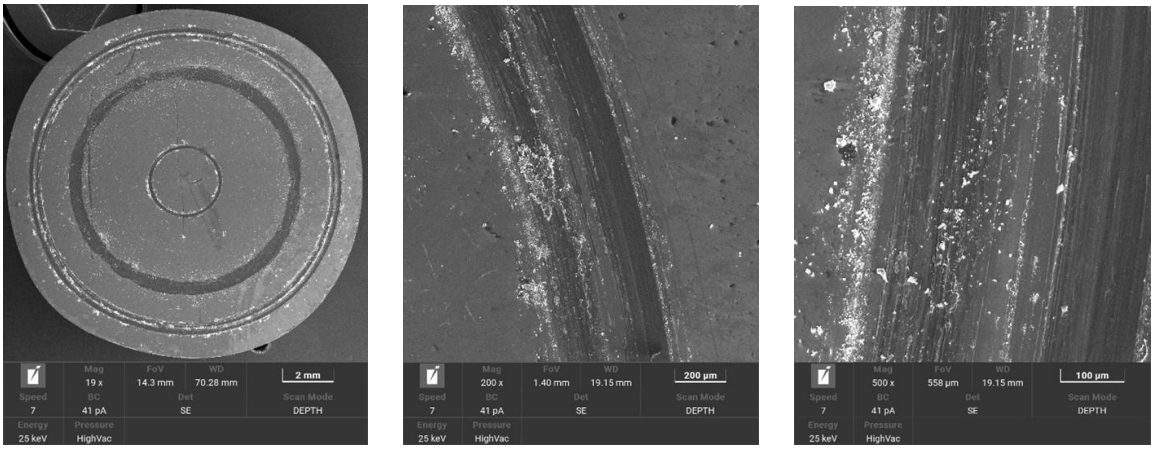

a) b) c)

Fig. 15. The surface of the Ti13Nb13Zr alloy with the SnO_2 coating modified by the PVD method coating after the friction pair abrasion test: Ti13Nb13Zr+SnO_2-steel ball, with SEM magnifications of a) 19×, b) 200×, and c) 500×

Wettability

Due to the application of the coating, a change occurred in the nature of the surface and the contact angle. The average values of the contact angle for the tested samples using distilled water are presented in Fig. 16. The noticeable differences in the contact angle values are dependent on the various properties of the liquid selected for the test. A 90° contact angle differentiates biomaterials considered hydrophilic or hydrophobic based on the adherence of the cells, which influenced the appearance of the droplets during the test (Fig. 16). In the case of the initial state Ti13Nb13Zr sample – the wetting angle is not changed by the character of the surface. In the case of the samples with coatings, the surface remained hydrophilic, with contact angles ranging from 0–90°. Obtaining a hydrophilic surface is closely related to the potential for proliferation and osseointegration, and such a surface remained despite the application of the coatings.

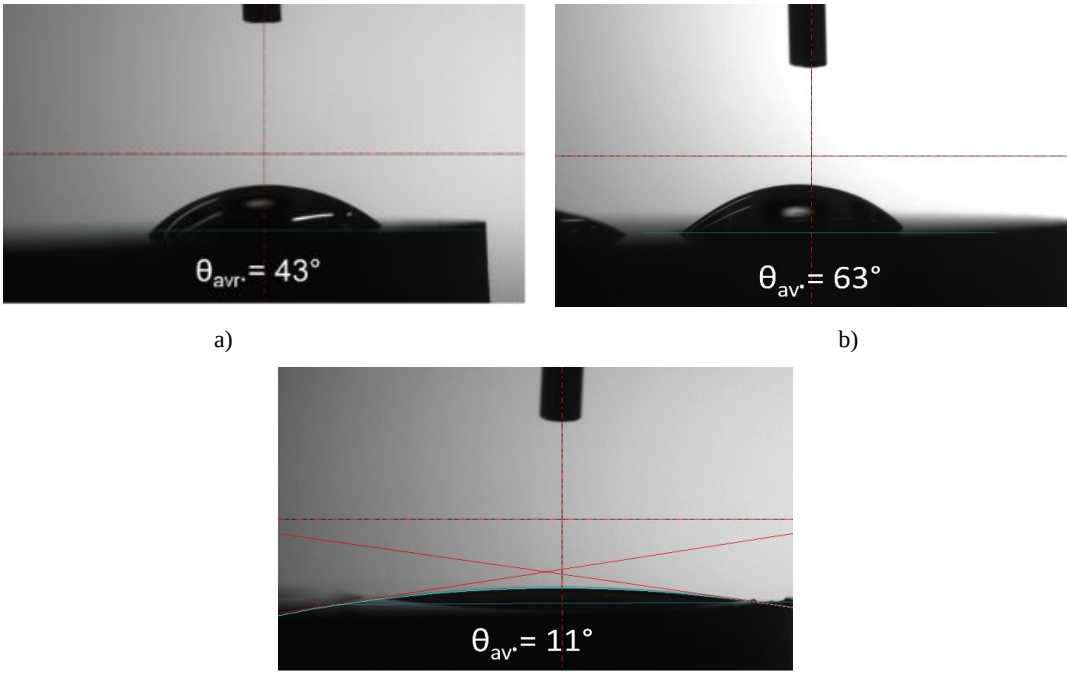

a) b) c)

Fig. 16. Contact angle images were taken during the wettability measurements for the: a) initial state Ti13b13Zr, b) Ti13Nb13Zr+SnO_2_ALD, and c) Ti13Nb13Zr+SnO_2_PVD samples

4. Discussion

To improve the antibacterial properties of a Ti13Nb13Zr alloy, thus reducing the adverse effects of any bacterial biofilm formation, a modification involving the application of a SnO_2 coating using the ALD or PVD methods was proposed. To ensure the required physicochemical properties of the Ti13Nb13Zr surface, certain surface treatment conditions were developed. The proposed surface treatment involved two consecutive processes: grinding on different gradation papers and then polishing in the next stage. In the final stage, the SnO_2 coating was applied using ALD. The variable parameters employed included a deposition temperature of 100 °C and 500 cycles. In the case of the applied SnO_2 coating, argon was used to generate the plasma for thin film deposition by vapor deposition. The gas was introduced at a power rate of 25%. First, the pitting corrosion resistance and EIS were tested using the potentiodynamic method, which produced polarization curves for the analysis. The SnO_2 coating applied using the ALD method slightly improved the electrochemical properties of the Ti13Nb13Zr alloy. Similar observations were noted by others [10] where surface modification via the ALD method to produce a ZnO coating improved polarization resistance. Furthermore, Kierat et al. [7] showed that the coating improves the corrosion resistance of the material. Others reported that a weak adherence of the inner coating to the surface can worsen corrosion resistance [14].

As part of the evaluation of the mechanical properties of the surface-modified Ti13Nb13Zr alloy, tests evaluating the adhesion to the substrate and abrasion resistance were performed. The obtained results showed that the applied coating is characterized by an improved adhesion in the case of samples subjected to the ALD process. Additionally, scratch tests have also been performed [15]. In this one, registered changes in acoustic emission were recorded. This type of cracking is visible in the form of local delaminations (Lc_1, Lc_2), not complete destruction of Lc_3, such as the cracking found in our research. On the other hand, the abrasion resistance tests have shown a significant influence of the applied SnO_2 coating on the Ti13Nb13Zr alloy by the ALD method compared to the substrate material. In the case of the Al_2O_3 ball, the mean coefficient of friction was about 4 times lower than the initial state Ti13Nb13Zr. Others reported similar results where the mean coefficient of friction decreased after surface modification by diamond-coating compared to the initial substrate. Moreover, similar observations have been reported where the untreated surface had higher friction coefficients than modified surfaces [6].

The final stage of the research was the surface wettability assessment. For each analyzed variant, the hydrophilic nature of the surface was observed. Greater wettability, i.e., a smaller contact angle, favors the adhesion of cells to the surface of the biomaterial, which is especially important in the case of orthopedic implants, as it affects the process of integrating the implant into the tissue. Similar results were observed by others, where the water contact angle decreased after surface modification compared to the initial state sample. Importantly, both samples were hydrophilic [6].

5. Conclusions

The obtained data showed different physicochemical properties of antibacterial films generated under various parameters in the case of temperature and number of cycles in the ALD process. These results directly assist in the optimization of the SnO_2 coating creation process using ALD-based methods on the surfaces of Ti13Nb13Zr alloy implants intended for the skeletal system, thus improving their functional properties. Applying a SnO_2 coating did not deteriorate the resistance of the Ti13Nb13Zr alloy to pitting corrosion and did not affect other potentiodynamic properties. Moreover, the application of a SnO_2 coating enabled good adhesion of the coating to the substrate (Ti13Nb13Zr alloy). Furthermore, applying a SnO_2 coating reduced the friction coefficient, thereby improving the abrasion resistance of the Ti13Nb13Zr alloy, which promotes its use in the skeletal system. Similarly, the application of a SnO_2 coating did not change the surface character of the Ti13Nb13Zr alloy. The surface remained hydrophilic, which increased the process of osseointegration and cell proliferation. The obtained results can be used as a basis to develop more detailed criteria for the final quality of medical devices which will ensure the required biocompatibility of implants and in this way have contributed to decreasing the risk of mineralization in postoperative complications. The results have increased effectiveness, decreased complication indicators, and improved the lives of patients.

Acknowledgements

Research funded by:

Statutory activities of Department of Biomaterials and Medical Devices Engineering, Faculty of Biomedical Engineering, Silesian University of Technology no. 07/020/BKM_22/0075.

The project was funded by the National Science Centre, Poland allocated based on the decision No. 2018/29/B/ST8/02314.

The project was funded by the Excellence Initiative – Research University programme allocated on the basis of the decision No. 32/014/SDU/10-22-16.

References

[1] ARAVINDAN V., JINESH K.B., PRABHAKAR R.R., KALE V.S., MADHAVI S., *Atomic layer deposited (ALD) SnO_2 anodes with exceptional cycleability for Li-ion batteries*, Nano Energy, 2013, 2, 720–725, DOI: 10.1016/j.nanoen.2012.12.007.

[2] BANSAL P., SINGH G., SIDHU H.S., *Improvement of surface properties and corrosion resistance of Ti13Nb13Zr titanium alloy by plasma-sprayed HA/ZnO coatings for biomedical applications*, Mater. Chem. Phys., 2021, 30 (3), 257, DOI: 10.1016/j.matchemphys.2020.123738.

[3] BANSAL P., SINGH G., SIDHU H.S., *Plasma-Sprayed Hydroxyapatite-Strontium Coating for Improved Corrosion Resistance and Surface Properties of Biodegradable AZ31 Mg Alloy for Biomedical Applications*, J. Mater. Eng. Perform., 2021, 30, 1768–1779, DOI: 10.1007/s11665-021-05490-0.

[4] BHALSHANKAR S., *Application of Nano Technology*, [in:] Biomedical Engineering EasyChair, 2021.

[5] HACKING S.A., ZURAW M., HARVEY E.J., TANZER M., KRYGIER J.J., BOBYN J.D., *A physical vapor deposition method for controlled evaluation of biological response to biomaterial chemistry and topography*, J. Biomed. Mater. Res., Part A, 2007, 82 (1), 179–187, https://doi.org/10.1002/jbm.a.31131

[6] HUSSEIN M.A., YILBAS B., KUMAR A.M., DREW R., AL--AQEELI N., *Influence of Laser Nitriding on the Surface and Corrosion Properties of Ti-20Nb-13Zr Alloy in Artificial Saliva for Dental Applications*, J. Mater. Eng. Perform., 2018, 27 (9), 4655–4664, https://doi.org/10.1007/s11665-018-3569-2

[7] KIERAT O., DUDEK A., ADAMCZYK L., *The effect of the corrosion medium on silane coatings deposited on titanium grade 2 and titanium alloy Ti13Nb13Zr*, Mater., 2022, 14 (21), https://doi.org/10.3390/ma14216350

[8] KOPOVA I., STRÁSKÝ J., HARCUBA P., LANDA M., JANEČEK M., BAČÁKOVA L., *Newly developed Ti–Nb–Zr–Ta–Si–Fe biomedical beta titanium alloys with increased strength and enhanced biocompatibility*, Mater. Sci. Eng. C, 2016, 60, 230–238, https://doi.org/10.1016/J.MSEC.2015.11.043

[9] KURODA D., NIINOMI M., MORINAGA M., KATO Y., YASHIRO T., *Design and mechanical properties of new β type titanium alloys for implant materials*, Mater. Sci. Eng. A, 1998, 243 (1–2), 244–249, https://doi.org/10.1016/S0921-5093(97)00808-3.

[10] LISOŃ J., TARATUTA A., PASZENDA Z., DYNER M., BASIAGA M., *A study on the physicochemical properties of surface modified Ti13Nb13Zr alloy for skeletal implants*, Acta Bioeng. Biomech., 2022, 24 (1), 39–47, DOI: 10.37190/ABB-01919-2021-04.

[11] LIU X., CHU P.K., DING C., *Surface modification of titanium, titanium alloys, and related materials for biomedical applications*, Mater. Sci. Eng. R Rep., 2004, 47 (3–4), 49–121, https://doi.org/10.1016/J.MSER.2004.11.001

[12] MORINAGA M., KATO M., KAMIMURA T., FUKUMOTOM M., HARADA I., KUBO K., *Theoretical design of β-type titanium alloys*, Titanium 1992, Science and Technology, Proc. 7th Int. Conf. on Titanium, San Diego, CA, USA, June 29–July 2, 1992, 276–283.

[13] NIINOMI M., LIU Y., NAKAI M., LIU H., LI H., *Biomedical titanium alloys with Young's moduli close to that of cortical bone*, Regen. Biomater., 2016**,** 3 (3), 173–185, https://doi.org/10.1093/rb/rbw016

[14] PAWŁOWSKI Ł., ROŚCISZEWSKA M., MAJKOWSKA-MARZEC B., JAŻDŻEWSKA M., BARTMAŃSKI M., ZIELIŃSKI A., TYBUSZEWSKA N., SAMSEL P., *Influence of Surface Modification of Titanium and Its Alloys for Medical Implants on Their Corrosion Behavior*, Mater., 2022, 15 (21), 7556, https://doi.org/10.3390/ma15217556

[15] PIOTROWSKA K., GRANEK A., MADEJ M., *Assessment of Mechanical and Tribological Properties of Diamond-Like Carbon Coatings on the Ti13Nb13Zr Alloy*, Open Eng., 2020, 10 (1), 536–545, https://doi.org/10.1515/eng-2020-0043.

[16] QUINN J., MCFADDEN R., CHAN C.W., CARSON L., *Titanium for Orthopedic Applications: An Overview of Surface Modification to Improve Biocompatibility and Prevent Bacterial Biofilm Formation*, iScience, 2020, 23 (11), 101745, DOI: 10.1016/j.isci.2020.101745.

[17] SEMLITSCH M., STAUB F., WEBER H., *Titanium-Aluminium-Niobium Alloy, Development for Biocompatible, High Strength Surgical Implants – Titan-Aluminium-Niob-Legierung, entwickelt für körperverträgliche, hochfeste Implantate in der Chirurgie"*, BMT, 2009, 30 (12), 334–339, https://doi.org/10.1515/bmte.1985.30.12.334